The Use of GPS for Vehicle Stability Control Systems

Robert Daily and David M. Bevly

***Abstract*—This paper presents a method for using global positioning system (GPS) velocity measurements to improve vehicle lateral stability control systems. GPS can be used to calculate the sideslip angle of a vehicle without knowing the vehicle model. This measurement is combined with other traditional measurements to control the lateral motion of the vehicle. Noise estimates are provided for all measurement systems to allow the sensors to be accurately represented. Additionally, a method to calculate the lateral forces at the tires is presented. It is shown that the tire estimation algorithm performs well outside the linear region of the tire. Results for the controller and force calculations are shown using a nonlinear model to simulate the vehicle and the force calculations are validated with experimental measurements on a test vehicle.**

***Index Terms*—Global positioning system (GPS), lateral stability, road vehicle control, vehicle dynamic control.**

I. Introduction

MANY VEHICLE control systems, including stability control and lateral position control, require measurements of yaw rate and vehicle slip angle [1]. The yaw rate can easily be measured by a gyro. Typically, the vehicle slip angle is either estimated with an observer integrating the gyro and knowing the vehicle model [2], by using accelerometers and integrating the lateral and longitudinal acceleration to determine the velocity [3], [4] or some combination of the two [5]. These methods have drawbacks due to errors arising from model and sensor uncertainties.

The global positioning system (GPS) allows the vehicle slip angle to be determined without requiring a model of the system. GPS does have several drawbacks. The sample rate of most GPS receivers is 10 Hz, which is much lower than the typical sample rates of accelerometers and gyros. Additionally, the GPS measurement contains higher noise than traditional inertial sensors. This paper will show it is possible to utilize the advantages of GPS while working within its limitations to accurately control a vehicle. GPS has already proved effective when used for vehicle navigation [6], [7] and lane keeping [8] as well as estimating cornering stiffness [9] and wheel slip [10]. GPS has also been used to measure yaw rate [11].

The goal of most lateral vehicle stability control systems is to control the vehicle's yaw rate or slip angle. There are several papers that present methods for controlling slip angle and yaw rate [12]. The thrust of this paper is not to present a new method for controlling the vehicle, but to show that GPS measurements can be used to enhance existing control methods.

Manuscript received February 14, 2003; revised November 1, 2003. Abstract published on the Internet January 13, 2004.

The authors are with the Department of Mechanical Engineering, Auburn University, Auburn, AL 36849 USA (e-mail: dailyrl@auburn.edu).

Digital Object Identifier 10.1109/TIE.2004.824851

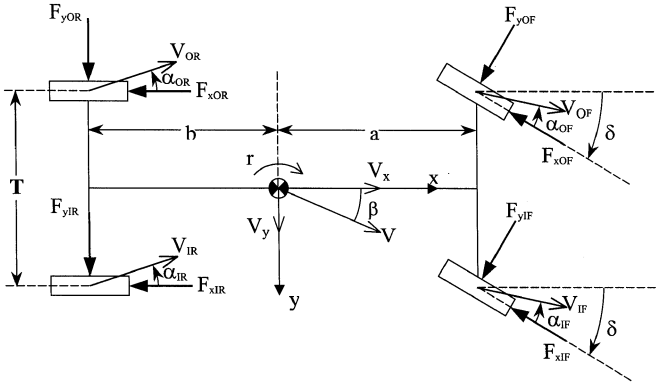

Fig. 1. Model of system.

There are two main ways to control the lateral motion of a vehicle. The first is to directly control the steer angle (steer-by-wire) [13], [14]; the second is to control the longitudinal force generated at each wheel (differential braking) [15]. Steer-by-wire is more widely used for autonomous control of a vehicle because most drivers would feel uncomfortable without a direct mechanical link between the steering wheel and the tires. Differential braking is the method usually employed in vehicle stability control systems. A problem arises, however, when choosing how to split the braking force among the four tires. With GPS it is possible to determine the slip angle instead of estimating it, therefore, accurate calculation of the tire curve is possible. These forces can be taken into account to optimize the braking force division without saturating a particular tire before the others.

II. Equations of Motion

Fig. 1 shows a schematic of a vehicle.

The lateral dynamics of the vehicle are described by

$$\begin{aligned}\dot{\beta} &= \frac{(F_{yIR}+F_{yOR})+(F_{yIF}+F_{yOF})\cos\delta-(F_{xIF}+F_{xOF})\sin\delta}{mV\cos\beta} - \frac{\dot{V}\tan\beta}{V} - r \\ \dot{r} &= \frac{a[(F_{yIF}+F_{yOF})\cos\delta-(F_{xIF}-F_{xOF})\sin\delta]-b(F_{yIR}+F_{yOR})}{I_z} \\ &\quad + \frac{\frac{T}{2}[(F_{yIF}-F_{yOF})\sin\delta+(F_{xIR}-F_{xOR})+(F_{xIF}-F_{xOF})\cos\delta]}{I_z}.\end{aligned} \tag{1}$$

The Pacejka tire model [16] shown in Fig. 2 is used to calculate the lateral forces at the tires (F_y). In this tire model, the lateral

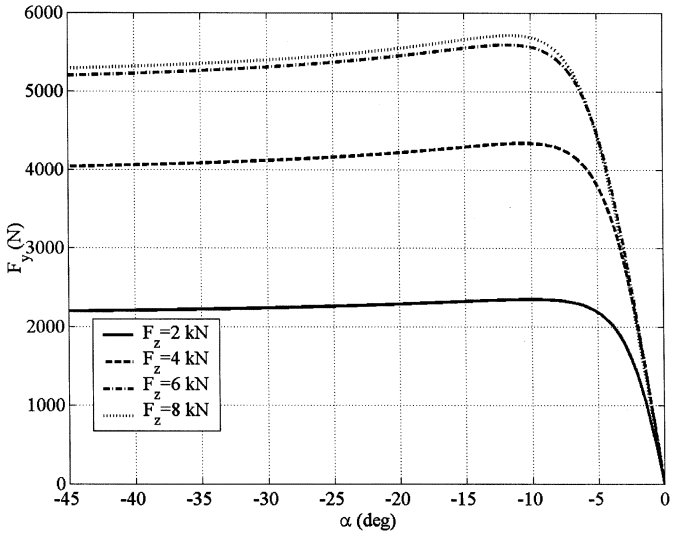

Fig. 2. Pacejka tire model for various loading cases.

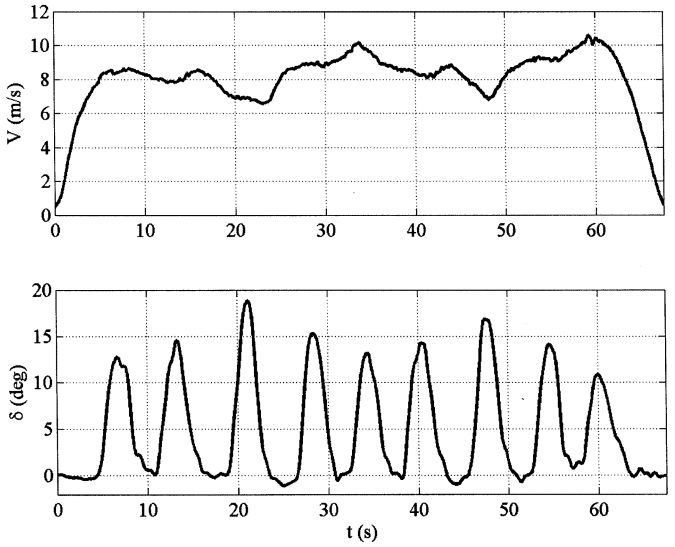

Fig. 3. Measured input into vehicle.

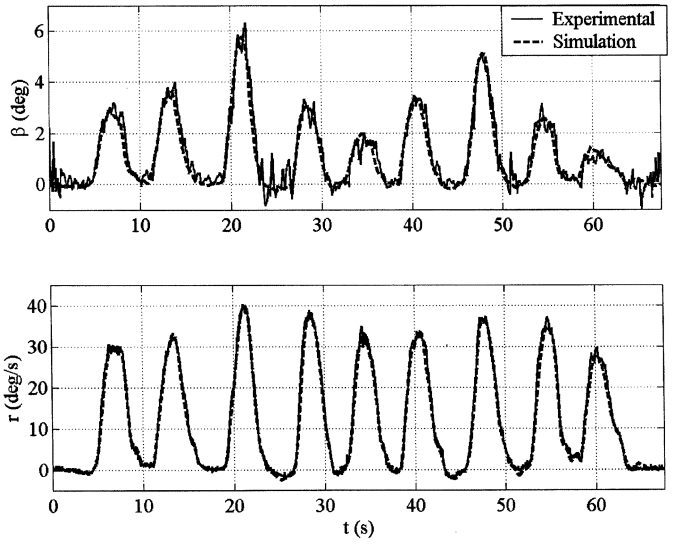

Fig. 4. Comparison of yaw rate and slip angle.

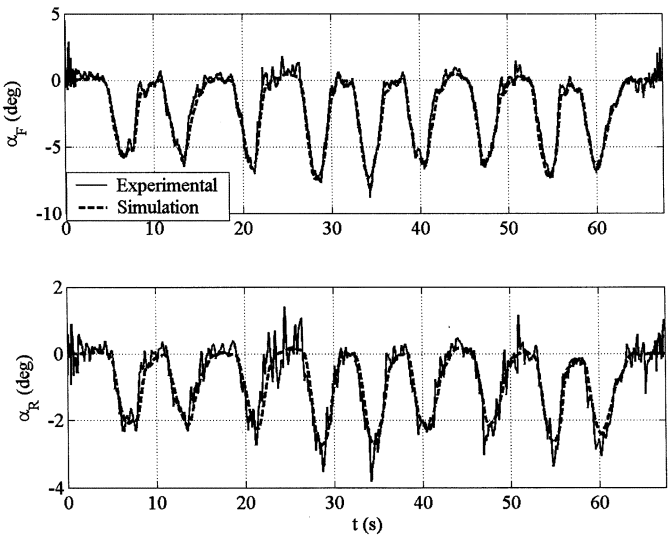

Fig. 5. Comparison of tire slip angles.

forces are calculated from the vertical load and slip angle at the tire. The vertical force (F_z) at the tire is simply the static weight on the tire plus the contribution from lateral weight transfer. The slip angle at the tire (α) is calculated by

$$\alpha_{IF} = \tan^{-1}\left(\frac{V\sin\beta + ar}{V\cos\beta - \frac{T}{2}r}\right) - \delta$$
$$\alpha_{IR} = \tan^{-1}\left(\frac{V\sin\beta - br}{V\cos\beta - \frac{T}{2}r}\right)$$
$$\alpha_{OF} = \tan^{-1}\left(\frac{V\sin\beta + ar}{V\cos\beta + \frac{T}{2}r}\right) - \delta$$
$$\alpha_{OR} = \tan^{-1}\left(\frac{V\sin\beta - br}{V\cos\beta + \frac{T}{2}r}\right). \quad (2)$$

Fig. 3 shows the velocity and steer angle input of an experiment performed in a parking lot using a Chevrolet Blazer. Steer angle is measured using a string potentiometer, and velocity is measured with GPS.

Figs. 4 and 5 show the resulting yaw rate, sideslip angle, and tire slip angles determined using GPS velocity measurements and a yaw rate gyroscope. The front and rear slip angles are averaged over the inner and outer tires. The method to determine sideslip experimentally is presented in the next section. The figures also contain the output from the dynamic model given in (1) and (2).

III. Measurements and Limitations

As was previously mentioned, the vehicle sideslip angle can be determined experimentally using the GPS velocity measurement and a yaw rate gyroscope. This is done by taking the difference of the GPS velocity heading (ψ_{GPS}) and the gyro heading (ψ_{gyro}).

$$\beta = \psi_{\mathrm{gyro}} - \psi_{\mathrm{GPS}}. \quad (3)$$

The gyro heading is found by integrating the yaw rate gyroscope during a turn. During straight driving, the gyro heading bias is eliminated to minimize error from the integrated gyroscope.

The effects of latency must also be taken into account. It is important to make sure each of the measurements is for the same moment in time. Because the expected slip angles are reasonably small (3°–7°), any difference in time could cause a noticeable error in the slip angle calculation. Every GPS measurement includes a time stamp, which allows the measurements to be aligned correctly and to not introduce latency errors [9].

In this paper, error or accuracy refers to the 1σ standard deviation of the stochastic errors. A gyro is used to measure the vehicle's yaw rate. The yaw rate gyro used in this work had an accuracy of $0.05°/\text{s}$. As the previous section stated (3), vehicle sideslip angle is the difference in the GPS heading and the integrated yaw rate gyro heading. Assuming a well-calibrated gyroscope over short integration times, the vehicle sideslip angle error is dominated by the error in the GPS velocity measurement [10].

A single GPS receiver can measure velocity very accurately in one of two methods. The receiver either measures the Doppler shift of the GPS carrier wave, or measures the carrier phase difference between two consecutive samples to determine velocity. These methods provide more accuracy than simple differentiating the GPS position measurement. Typical GPS receivers can measure velocity with an accuracy of 5 cm/s. [10]

Slip angle is calculated by

$$\beta + \beta_{\text{error}} = \tan^{-1}\left(\frac{V_y + V_{\text{yerror}}}{V + V_{\text{error}}}\right) \approx \frac{V_y + V_{\text{yerror}}}{V + V_{\text{error}}} \approx \frac{V\beta + V_{\text{yerror}}}{V + V_{\text{error}}}. \quad (4)$$

Therefore, the slip angle error can be approximated as

$$\beta_{\text{error}} \approx \frac{V_{\text{yerror}}}{V}. \quad (5)$$

Using GPS velocity measurements, this leads to the vehicle slip angle accuracy (σ_β) as a function of the GPS velocity accuracy (σ_V)

$$\sigma_\beta = \frac{\sigma_V}{V}. \quad (6)$$

A Monte Carlo simulation is used to verify the vehicle slip angle error. As Fig. 6 shows, analytical vehicle slip angle errors given in (6) match the Monte Carlo simulation.

By a similar derivation, the accuracy of the tire slip angles ($\sigma_{\alpha F}$, $\sigma_{\alpha R}$) can be calculated using

$$\sigma_{\alpha F} = \frac{\sigma_V + a\sigma_r}{V}\ \sigma_{\alpha R} = \frac{\sigma_V + b\sigma_r}{V}. \quad (7)$$

For realistic yaw rate accuracies, the gyro noise (σ_r) in (7) is much less than the GPS velocity noise (σ_V). Therefore, the accuracy of the tire slip angle is virtually the same as the accuracy of the vehicle slip angle.

The experimental data presented in the previous section (Figs. 3–5) was run at an average velocity of 8 m/s. Equation (6) leads to an expected error on the vehicle slip angle (and, hence, the tire slip angles) of 0.36°. The low frequency errors arising from unmodeled vehicle dynamics were removed using a high-pass filter with a very low cutoff frequency. The resulting higher frequency errors representing the measurement noise are shown in Fig. 7.

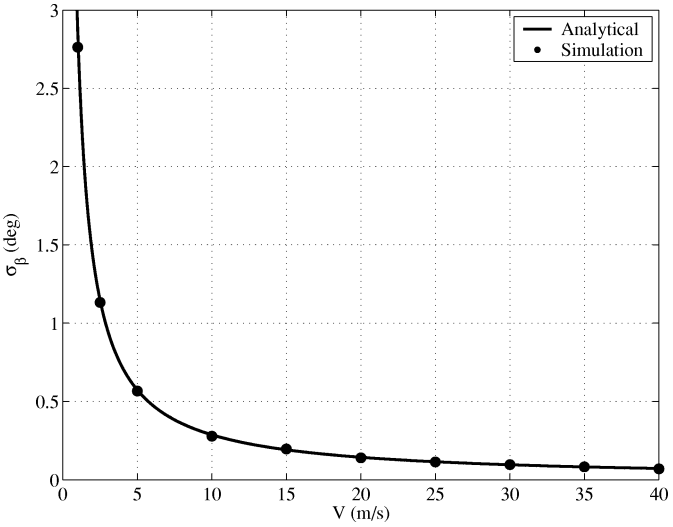

Fig. 6. Slip angle accuracy.

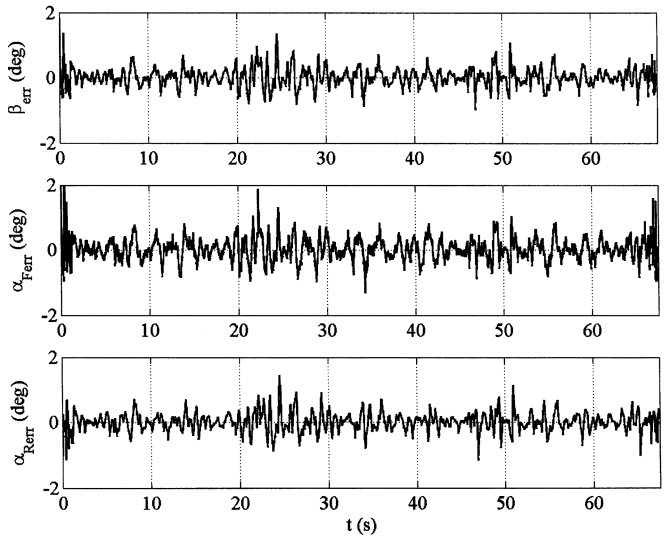

Fig. 7. Experimental measurement noise.

The standard deviation of the noise on the vehicle slip angle is 0.27°. On the front and rear slip angles it is 0.33° and 0.27°, respectively. This noise fits very well with the expected error using (6) and (7).

To simulate realistic measurements the noise characteristics developed in this section are added to the output of the dynamic equations from the previous section. Additionally, the output of the simulation is recorded at 10 Hz, matching the sample rate of a typical GPS receiver.

IV. Steering Controller Development

The controller developed in this section regulates the steer angle. As the introduction stated, this method is not regularly used for vehicle stability control systems; however, it is used to autonomously drive vehicles or for lane keeping maneuvers and can be used to demonstrate the feasibility of using GPS

measurements for vehicle control. It also has more capability than differential braking in recovering from unstable situations [14], [17].

While the nonlinear system developed previously simulates the vehicle, a simpler model is utilized to develop the vehicle controller. The system is linearized, weight transfer is neglected, velocity is assumed constant, and the inner and outer tire slip angles are assumed equal. In addition, lateral force at each tire is assumed linear

$$F_y = C_\alpha \alpha. \tag{8}$$

with $C_{\alpha F}$ and $C_{\alpha R}$ the combined cornering stiffness of the front and rear axles, respectively.

These assumptions lead to (9), known as the bicycle model

$$\begin{bmatrix} \dot{\beta} \\ \dot{r} \end{bmatrix} = \begin{bmatrix} -\frac{C_{\alpha F}+C_{\alpha R}}{mV} & -\frac{aC_{\alpha F}-bC_{\alpha R}}{mV^2} - 1 \\ -\frac{aC_{\alpha F}-bC_{\alpha R}}{I_z} & -\frac{a^2C_{\alpha F}+b^2C_{\alpha R}}{I_z V} \end{bmatrix} \begin{bmatrix} \beta \\ r \end{bmatrix} + \begin{bmatrix} \frac{C_{\alpha F}}{mV} \\ \frac{aC_{\alpha F}}{I_z} \end{bmatrix} \delta. \tag{9}$$

Equation (9) is represented in a more general form in (10) or in discrete form in (11)

$$\dot{\boldsymbol{x}} = \boldsymbol{A}x + \boldsymbol{B}u \tag{10}$$

$$\boldsymbol{x}^{(i+1)} = \boldsymbol{A}_D \boldsymbol{x}^{(i)} + \boldsymbol{B}_D u^{(i)}. \tag{11}$$

By applying state feedback ($u^{(i)} = -\boldsymbol{K}\boldsymbol{x}^{(i)}$) and equating the eigenvalues of the desired and actual systems in state-space form (12), $\boldsymbol{K}$ is obtained

$$\operatorname{eig}(\boldsymbol{A}_{D\mathrm{des}}) = \operatorname{eig}(\boldsymbol{A}_D - \boldsymbol{B}\boldsymbol{K}). \tag{12}$$

Additionally, a reference input ($\boldsymbol{x}_{\mathrm{des}}$) is generated using the steady-state values of the desired system (13)

$$\boldsymbol{x}_{\mathrm{des}}^{(i)} = \boldsymbol{A}_{\mathrm{des}}^{-1} \boldsymbol{B}_{\mathrm{des}} \delta^{(i)}. \tag{13}$$

The desired system ($\boldsymbol{A}_{\mathrm{des}}, \boldsymbol{B}_{\mathrm{des}}$) is taken to be a vehicle with $3^\circ/\mathrm{g}$ of understeer. Understeer (K_{US}) is defined as

$$K_{US} = \frac{W_F}{C_{\alpha F}} - \frac{W_R}{C_{\alpha R}}. \tag{14}$$

The understeer is changed by modifying the weight split.

Next, a gain ($\bar{N}$) for the reference input is developed

$$\begin{bmatrix} \boldsymbol{N}_x \\ N_u \end{bmatrix} = \begin{bmatrix} \boldsymbol{A}_D - \boldsymbol{I} & \boldsymbol{B}_D \\ \boldsymbol{C}_D & 0 \end{bmatrix}^{-1} \begin{bmatrix} \mathbf{o} \\ 1 \end{bmatrix} \tag{15}$$

$$\bar{N} = N_u + \boldsymbol{K}\boldsymbol{N}_x \tag{16}$$

where setting $\mathbf{C}_D = [1 \quad 0]$ controls β, and setting $\boldsymbol{C}_D = [0 \quad 1]$ controls r. The control input (u) is generated by combining the feedback and reference input [18]

$$u^{(i)} = -\mathbf{K}\hat{\mathbf{x}}^{(i)} + \bar{N}\mathbf{C}_D \mathbf{x}_{\mathrm{des}}^{(i)}. \tag{17}$$

Since GPS measurements are only sampled at 10 Hz, the eigenvalues of the desired system are limited in order to keep the natural frequency below half of the controller bandwidth. Fig. 8 shows the poles of the desired system ($3^\circ/\mathrm{g}$ of understeer) as well as an uncontrolled system with $1^\circ/\mathrm{g}$ of oversteer at 10 and 20 m/s.

The controller response is tested with a step steer input. In this test, the uncontrolled system has $1^\circ/\mathrm{g}$ of oversteer and is run at 20 m/s. Fig. 9 depicts the uncontrolled system's behavior.

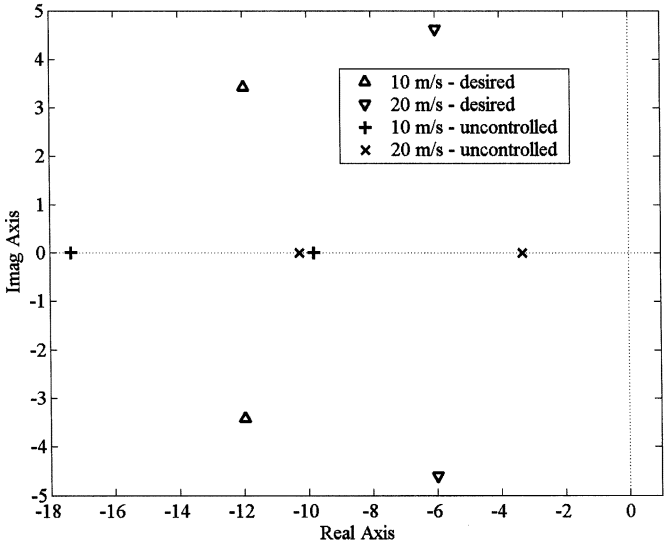

Fig. 8. Poles of desired and uncontrolled system.

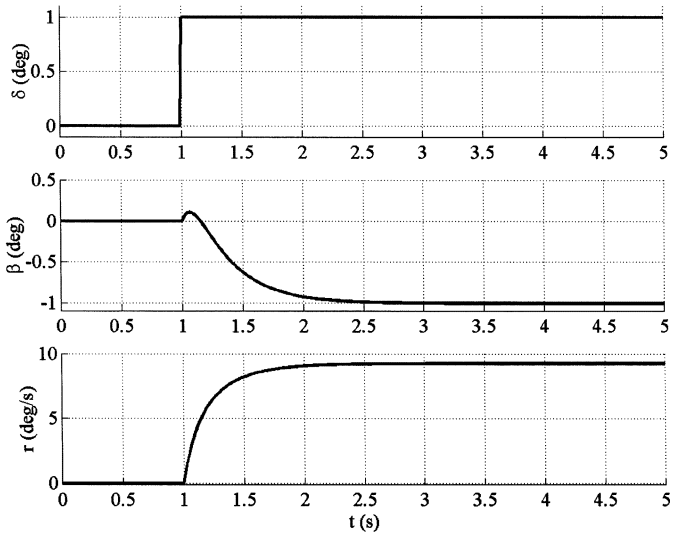

Fig. 9. Uncontrolled system response.

Fig. 10 shows the response of the controlled system when yaw rate is being controlled. The apparent noise on the steer angle is not noise, but the controller's response to noisy measurements. As the figure shows, the vehicle dynamics filter most of this noise out so it is not very apparent in the system response.

V. Braking Controller Development

In most vehicle stability control systems differential braking is used as the control actuator instead of steering [19], [20]. This section presents a method to control the vehicle through differential braking. The steering input from the driver is still applied, however braking is applied to supplement the driver's input.

As with the steering control, a linear system is used to control the vehicle. The state-space bicycle model (10) is modified to include longitudinal forces at each tire

$$\dot{\boldsymbol{x}} = \boldsymbol{A}x + \boldsymbol{B}_1 \boldsymbol{u}_1 + \boldsymbol{B}_2 u_2. \tag{18}$$

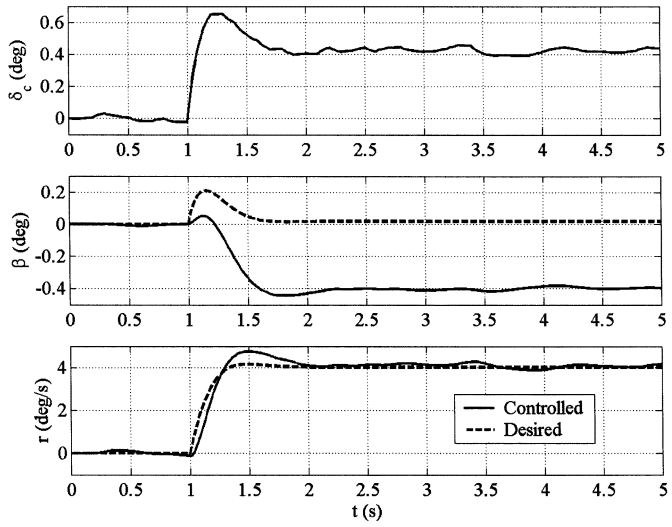

Fig. 10. Controlled steering system response.

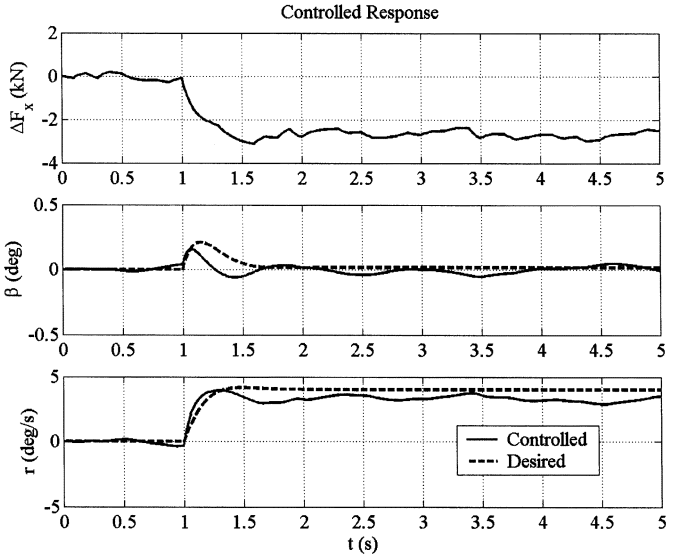

Fig. 11. Controlled braking system response.

with

$$\boldsymbol{A} = \begin{bmatrix} -\frac{C_{\alpha F}+C_{\alpha R}}{mV} & -\frac{aC_{\alpha F}-bC_{\alpha R}}{mV^2}-1 \\ -\frac{aC_{\alpha F}-bC_{\alpha R}}{I_z} & -\frac{a^2C_{\alpha F}+b^2C_{\alpha R}}{I_zV} \end{bmatrix}$$

$$\boldsymbol{B}_1 = \begin{bmatrix} \frac{C_{\alpha F}}{mV} & \frac{-1}{mV} \\ \frac{aC_{\alpha F}}{I_z} & \frac{a}{I_z} \end{bmatrix} \boldsymbol{B}_2 = \begin{bmatrix} 0 \\ \frac{T}{2I_z} \end{bmatrix}$$

$$\boldsymbol{u}_1 = \begin{bmatrix} \delta \\ (F_{xIF}+F_{xOF})\,\delta \end{bmatrix}$$

$$u_2 = (F_{xIF}-F_{xOF})+(F_{xIR}-F_{xOR})$$

or, in discrete form

$$\boldsymbol{x}^{(i+1)} = \boldsymbol{A}_D\boldsymbol{x}^{(i)} + \boldsymbol{B}_{1D}\boldsymbol{u}_1^{(i)} + \boldsymbol{B}_{2D}u_2^{(i)}. \tag{19}$$

As in the steering control, the desired response is determined by the driver's steering input applied to a vehicle with $3^\circ/\mathrm{g}$ of understeer. State feedback is again used to generate the controller. Due to the force terms (F_{xIF}, F_{xOF}) in $\boldsymbol{u}_1$ this term has a one step time lag. In order to compute the total input the driver's steer input $(\boldsymbol{u}_1)$ must be fed forward and combined with the control input (u_2). To accomplish this, equation (15) is modified

$$\begin{bmatrix} \boldsymbol{N}_x \\ N_u \end{bmatrix} = \begin{bmatrix} \boldsymbol{A}_D-\boldsymbol{I} & \boldsymbol{B}_D \\ \boldsymbol{C}_D & 0 \end{bmatrix}^{-1} \begin{bmatrix} \boldsymbol{d} \\ 1 \end{bmatrix} \tag{20}$$

with

$$\boldsymbol{d} = \frac{-\boldsymbol{B}_{1D}\boldsymbol{u}_1}{\boldsymbol{C}_D\boldsymbol{x}_{\mathrm{des}}}.$$

The control input is then developed by combining the state feedback with the reference input exactly as in the steering control (17).

The controller is tested using the same situation as the steering controller used in the previous section. A step steer input is provided by the driver. The uncontrolled system has $1^\circ/\mathrm{g}$ of oversteer and is run at 20 m/s. Fig. 11 shows the controlled response of the system. This case shows slip angle being controlled instead of yaw rate as was done in the steering control.

As with the steering controller, the controlled response matches the desired response very well. The slight deviation from zero in the response before the step steer input is applied is due to noise in the measurements.

VI. Calculating Lateral Forces

The controller presented previously uses differential braking as the control actuator to generate a torque about the vertical axis of the vehicle, thus causing the vehicle to yaw.

The braking control input, however, is $(F_{xIF}-F_{xOF})+(F_{xIR}-F_{xOR})$. This leads to the problem of how to split the braking force between the front and rear wheels as well as between inner and outer wheels. Ideally, the braking forces applied should act in a way that saturates each tire at the same time. The total force a can tire provide is given by

$$\sqrt{F_x^2+F_y^2} \le F_T \tag{21}$$

known as the friction circle. If a tire is using most of its available force in the lateral direction it will not have much force available to provide braking. Therefore, the lateral force and total force possible at each tire must be known to determine how much braking force can be applied at each tire. Additionally, the longitudinal force the tires are using to maintain the desired velocity must be taken into account.

Control schemes that use an observer to estimate the vehicle slip angle require an accurate model of the system. Many times a linear tire model is used to produce a linear observer. Because the tire's saturation point lies outside the linear region, a linear observer would not be able to accurately predict the peak lateral force. A nonlinear observer would require knowledge of the nonlinear characteristics of the tire, as well as must account for roll in the vehicle and how the roll and resulting weight transfer affect the tire model. As will be shown this weight transfer contributes significantly to changes in tire characteristics.

Using GPS and a gyroscope, the vehicle's sideslip, yaw rate, and velocity can be measured (as opposed to estimated). This means it is possible to calculate the lateral forces at each tire, capturing the nonlinear effects of the tire without knowing a model for the tire.

As was previously stated, the forces required to maintain the desired velocity must also be considered. Assuming a rear wheel drive vehicle, the total longitudinal force at the front tires is simply the sum of the braking forces applied at the front wheels. The total longitudinal force at the rear tires is what is required to overcome the braking and maintain the desired velocity. Therefore, the total longitudinal force at the rear wheels must be calculated along with the lateral forces.

The lateral forces as well as the total longitudinal force at the rear wheels can be found from analyzing the forces in Fig. 1 using Newton's equations

$$\begin{aligned} -F_{xR} - F_{xF}\cos\delta - F_{yF}\sin\delta &= ma_x \\ F_{yR} - F_{xF}\sin\delta + F_{yF}\cos\delta &= ma_y \\ a\left[F_{yF}\cos\delta - F_{xF}\sin\delta\right] - bF_{yR} + \frac{T}{2} & \\ \left[\Delta F_{xR} + \Delta F_{xF}\cos\delta - \Delta F_{yF}\sin\delta\right] &= I_z\dot{r}. \end{aligned} \tag{22}$$

with

$$\begin{aligned} F_{xF} &= F_{xIF} + F_{xOF} \quad F_{xR} = F_{xIR} + F_{xOR} \\ \Delta F_{xF} &= F_{xIF} - F_{xOF} \quad \Delta F_{xR} = F_{xIR} - F_{xOR} \\ F_{yF} &= F_{yIF} + F_{yOF} \quad F_{yR} = F_{yIR} + F_{yOR} \\ \Delta F_{yF} &= F_{yIF} - F_{yOF} \quad \Delta F_{yR} = F_{yIR} - F_{yOR}. \end{aligned}$$

Simultaneously solving the equations above and assuming the inner and outer lateral forces are the same leads to the solution for the lateral tire forces as well the total longitudinal force at the rear wheels

$$\begin{aligned} a_x &= \dot{V}\cos\beta - \left(\dot{\beta} + r\right)V\sin\beta \\ a_y &= V\left(\dot{\beta} + r\right)\cos\beta + \dot{V}\sin\beta \\ \begin{bmatrix} F_{xr} \\ F_{yF} \\ F_{yR} \end{bmatrix} &= \begin{bmatrix} 1 & \sin\delta & 0 \\ 0 & \cos\delta & 1 \\ 0 & a\cos\delta & -b \end{bmatrix}^{-1} \\ &\quad \cdot \begin{bmatrix} -ma_y - F_{xF}\cos\delta \\ ma_y + F_{xF}\sin\delta \\ I_z\dot{r} - \frac{T}{2}\left(\Delta F_{xR} + \Delta F_{xF}\cos\delta\right) + aF_{xF}\sin\delta \end{bmatrix}. \end{aligned} \tag{23}$$

Using a simple forward difference the derivatives of the vehicle's sideslip, yaw rate, and velocity can be approximated as

$$\begin{aligned} \dot{\beta}^{(i-1)} &= \frac{\beta^{(i)} - \beta^{(i-1)}}{t^{(i)} - t^{(i-1)}} \\ \dot{r}^{(i-1)} &= \frac{r^{(i)} - r^{(i-1)}}{t^{(i)} - t^{(i-1)}} \\ \dot{V}^{(i-1)} &= \frac{V^{(i)} - V^{(i-1)}}{t^{(i)} - t^{(i-1)}}. \end{aligned} \tag{24}$$

Since the derivatives are calculated using a forward difference, they are known only for the previous time step. Therefore, the forces are being estimated one time step behind the current time in the vehicle. The accelerations (a_x, a_y) can be calculated from the GPS velocities, or measured directly from accelerometers.

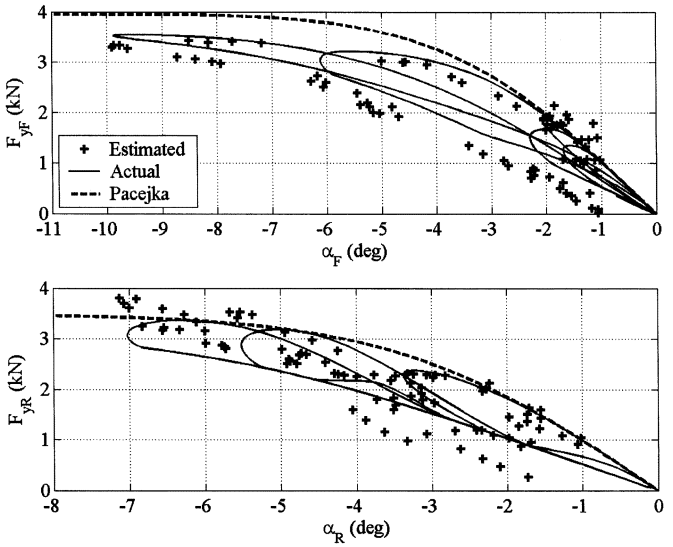

Fig. 12. Predicted tire curves.

Differentiating the GPS velocity measurements results in very noisy acceleration measurements and, therefore, noisy force calculations. This noise is calculated by

$$\sigma_a = \frac{\sigma_{V^{(i)} - V^{(i-1)}}}{T_s} = \frac{\sqrt{2}\sigma_V}{T_s} \tag{25}$$

with sample time T_s. With a sample rate of 10 Hz and the typical GPS velocity accuracy of 5 cm/s, the acceleration error from differentiating GPS velocity is 0.707 $\mathrm{m/s^2}$. A solution to the noisy force calculations is to use an accelerometer to measure the lateral acceleration directly. When a lateral accelerometer is used the effects of vehicle roll on the measurement must be taken out of the measurement. This can be done with a roll gyro, a second accelerometer, or using GPS. Once these effects are removed, the accelerometer measurement is very clean. Typical accelerometers have an error of 0.05 $\mathrm{m/s^2}$.

The goal of calculating the lateral forces is to produce lateral force vs. tire slip angle plots similar to the ones represented by the Pacejka tire model. This information can then be used to predict the tire's current lateral force and allow more intelligent stability control.

A common maneuver that generates high slip angles (where stability control might be needed) is the double lane change. This maneuver consists of changing to a neighboring lane and then immediately back again (normally to avoid an obstacle). This scenario is simulated to predict the tire curve. To create these plots an accelerometer is simulated to provide lateral acceleration measurements; longitudinal velocity is constant. Fig. 12 shows the actual force at the tire (from the nonlinear simulation), the calculated force using (23), and the Pacejka tire model force for static loading of the vehicle. Note that the true forces at the tires are significantly lower than the forces would be if no weight transfer were present. The lateral acceleration of the vehicle at the end of this simulation was 0.7 g (an extremely aggressive lane change). The front tires appear to be nearly saturated and the rear tires are close to saturation as well. The lateral force curves for no weight transfer, on the other hand, saturate at a higher lateral force, particularly on the front tire.

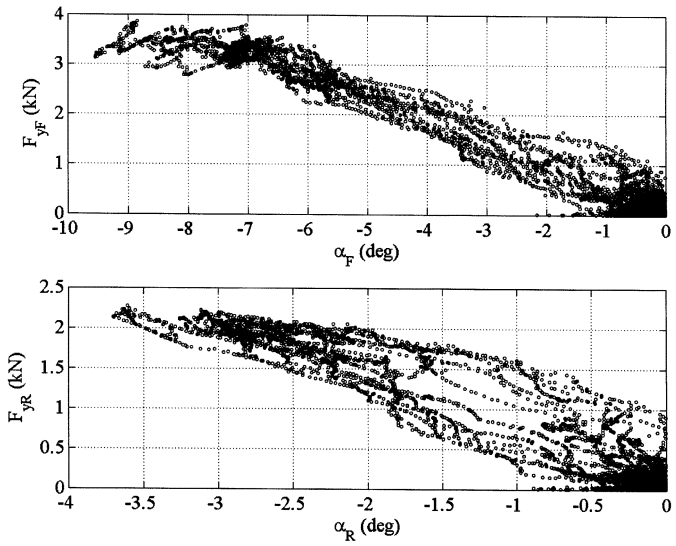

Fig. 13. Experimental tire curves.

The loops in the actual lateral force occur because the roll angle, and therefore weight transfer, of the vehicle is different entering and exiting the maneuver. This changes the lateral force dynamics as the vehicle performs the maneuver resulting in the loops on the tire curve.

The force/slip angle estimation is now applied to the experimental data in Section II producing the tire curves in Fig. 13. The looping of the tire curve can again be seen, particularly in the rear tire. The maneuver in the experiment was not as drastic as the simulation, so the tire curves are mainly in the linear region. However, as Fig. 12 shows the method is valid in the nonlinear region of the tire as well.

Knowing where a tire is on the tire curve, along with knowing the total longitudinal forces enables the controller to more accurately distribute the braking forces between the front and rear wheels. Care must also be taken to intelligently brake either the inner or the outer tire since acceleration of individual tires is not possible.

The controller presented in Section V divides the force so that the total force at each braking wheel (lateral force, braking force, and driving force) is a percentage of the maximum force available to that tire. This percentage is the same for the front and rear tires. Therefore, each braking tire hits 100% of its maximum force at the same time. In other words, the braking tires saturate at the same time and the maximum control input is applied.

VII. Conclusion

This paper has shown the feasibility of controlling a vehicle using GPS-based slip angle measurements. In reality, higher performance controllers can be developed using the GPS measurements combined with inertial sensors to provide higher update rate measurements [9]. Additionally, a method was presented to predict the lateral forces at each tire. These lateral forces can be used to optimally divide the braking forces among the tires when using differential braking to control the vehicle. Again, integrating GPS with traditional sensors (which still does not require a model of the vehicle) can provide performance beyond what is presented in this paper.

Further investigations are necessary to determine methods to intelligently divide the control input between steering and braking. Additional study into weight transfer phenomenon seen in the experimental tire curves is also warranted.

Acknowledgment

The authors would like to thank R. Anderson for instrumentation and use of his personal Chevrolet Blazer as well as collecting the data provided in this paper.

References

[1] S. Kimbrough, "Coordinated braking and steering control for emergency stops and accelerations," in *Proc. WAM ASME*, Atlanta, GA, 1991, pp. 229–244.

[2] U. Kiencke and A. Daiss, "Observation of lateral vehicle dynamics," in *Proc. 1996 IFAC*, pp. 7–10.

[3] V. Alberti and E. Babbel, "Improved driving stability by active braking on the individual wheel," in *Proc. Int. Symp. Advanced Vehicle Control*, June 1996, pp. 717–732.

[4] A. Hac and M. Simpson, "Estimation of vehicle side slip angle and yaw rate," presented at the SAE 2000 World Congr., Detroit, MI, Mar. 2000, Paper SAE 2000–01–0696.

[5] H. Nishio *et al.*, "Development of vehicle stability control system based on vehicle sideslip angle estimation," SAE, New York, SAE Paper 2001–01–0137, Mar. 2001.

[6] V. Morellas, T. Morris, L. Alexander, and M. Donath, "Preview based control of a tractor trailer using DGPS for road departure accidents," in *Proc. IEEE Conf. Intelligent Transportation Systems*, Boston, MA, Nov. 1997, pp. 797–805.

[7] E. Abbot and D. Powell, "Land-Vehicle navigation using GPS," *Proc. IEEE*, vol. 87, pp. 145–162, Jan. 1999.

[8] J. C. Gerdes and E. J. Rossetter, "A unified approach to driver assistance systems based on artificial potential fields," *Trans. ASME, J. Dyn. Syst., Meas., Control*, vol. 123, pp. 431–438, Sept. 2001.

[9] D. M. Bevly, R. Sheridan, and J. C. Gerdes, "Integrating INS sensors with GPS velocity measurements for continuous estimation of vehicle sideslip and tire cornering stiffness," in *Proc. 2001 American Control Conf.*, vol. 1, Arlington, VA, June 2001, pp. 25–30.

[10] D. M. Bevly, J. C. Gerdes, and C. Wilson, "The use of GPS based velocity measurements for measurement of sideslip and wheel slip," *Int. J. Veh. Mech. Mobility*, vol. 38, no. 2, pp. 127–147, August 2002.

[11] P. Y. Montgomery, H. Uematsu, and B. W. Parkinson, "Analysis of angular velocity determination using GPS," in *Proc. ION GPS 1994*, Salt Lake City, UT, 1994, pp. 697–706.

[12] K. J. Hunt, R. Haas, and J. C. Kalkkuhl, "Local controller network for autonomous vehicle steering," in *Proc. 13th Triennial World Congr.*, San Francisco, CA, 1996, pp. 405–410.

[13] K. T. Feng, H. S. Tan, and M. Tomizuka, "Automatic steering control of vehicle lateral motion with the effect of roll dynamics," in *Proc. American Control Conf.*, vol. 4, 1998, pp. 2248–2254.

[14] X. Tang and K. Yoshimoto, "Research of driver assistance system for recovering vehicle stability from unstable states," SAE, New York, SAE Paper 2001-01–1276, Mar. 2001.

[15] S. Matsumoto, H. Yamaguchi, H. Inoue, and Y. Yasuno, "Improvement of vehicle dynamics through braking force distribution control," SAE, New York, SAE Paper 920645, Feb. 1992.

[16] E. Bakker, L. Nyborg, and H. B. Pacejka, "Tyre modeling for use in vehicle dynamics studies," SAE, New York, SAE Paper 870421, Feb. 1987.

[17] S. R. Burns, R. T. O'Brien Jr, and J. A. Piepmeier, "Steering controller design using scale-model vehicles," in *Proc. Thirty-Fourth Southeastern Symp. System Theory*, Mar. 2002, pp. 476–478.

[18] G. F. Franklin, J. D. Powell, and M. Workman, *Digital Control of Dynamic Systems*, 3rd ed. Menlo Park, CA: Addison-Wesley Longman, 1997.

[19] T. Pilutti, G. Ulsoy, and D. Hrovat, "Vehicle steering intervention through differential braking," in *Proc. American Control Conf.*, vol. 3, June 1995, pp. 1667–1671.

[20] H. J. Kraft and H. Leffler, "The integrated brake and stability control system of the new BMW 850i," SAE, New York, SAE Paper 900209, Feb. 1990.

Robert Daily received the B.S. degree in 1999 from Auburn University, Auburn, AL, where he is currently working toward the Ph.D. degree.

His research interests include modeless control, parameter identification, adaptive control, and intelligent systems. He is currently researching unmanned ground vehicles and modifying vehicle behavior.

David M. Bevly received the B.S. degree from Texas A&M University, College Station, in 1995, the M.S. degree from Massachusetts Institute of Technology, Cambridge, in 1997, and the Ph.D. degree from Stanford University, Stanford, CA, in 2001, all in mechanical engineering.

In 2001, he joined the faculty of the Department of Mechanical Engineering, Auburn University, Auburn, AL, as an Assistant Professor. His research interests include control systems, sensor fusion, GPS, state estimation, and parameter identification. His research focuses on vehicle dynamics as well as modeling, navigation, and control of vehicle systems. Specifically, he has developed algorithms for control of off-road vehicles and methods for identifying critical vehicle parameters using GPS and inertial sensors.